THE JOURNAL OF PHYSICAL CHEMISTRY LETTERS
A JOURNAL OF THE AMERICAN CHEMICAL SOCIETY

pubs.acs.org/JPCL

Letter

Detuning Effects on the Reverse Intersystem Crossing from Triplet Exciton to Lower Polariton

Bin Zhang and Zhigang Shuai*

Cite This: *J. Phys. Chem. Lett.* 2022, 13, 9279−9286

Read Online

ACCESS | Metrics & More | Article Recommendations | Supporting Information

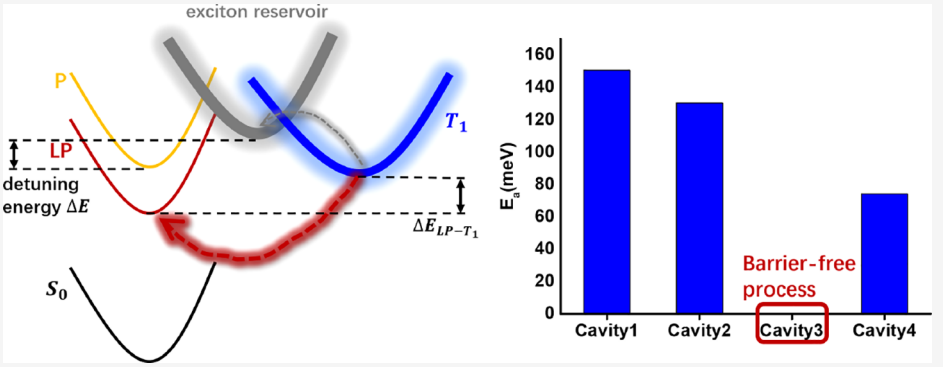

ABSTRACT: The lower polariton (LP) can reduce the energy barrier of the reverse intersystem crossing (rISC) process from T_1 to harvest triplet energy for fluorescence. Based on a Tavis−Cummings model including both singlet and triplet excitons, both coupled with quantized photons, we derive here a comprehensive rISC rate formalism. We found that the latter consists of three contributions: the one originated from spin−orbit coupling as first obtained by Martinez-Martinez et al. (*J. Chem. Phys.* **2019**, *151*, 054106), the one from light−matter coupling of Ou et al. (*J. Am. Chem. Soc.* **2021**, *143*, 17786), and the cross-term first reported here. We apply the formalism to investigate the experimentally observed barrier-free rISC (BFrISC) process in cavity devices with DABNA-2 molecular thin film. We found it can be attributed to the detuning effect. The rISC rates can be increased by orders of magnitude through changing the detuning energy to realize the BFrISC process. In addition, the BFrISC rates exhibit a maximum as a function of the incident angle and the doping concentration. The formalism provides a solid ground for molecular design toward highly efficient cavity-promoted light-emitting materials.

Electronic processes in organic functional materials have attracted increasing interest for understanding light emission,[1] photovoltaics,[2] thermo-electric conversion,[3] etc. Recently, a microcavity has been employed to investigate the number of chemical processes and physical properties including optical emission. When the molecules are constrained inside the cavity, the molecular exciton interacts strongly with confined electromagnetic fields of the cavity through a transition electric dipole to form hybridized light−matter states, the exciton polariton.[4−8] Such cavity polaritons have been applied in controlling chemical reactions,[9−12] in realizing long distance energy transfer,[13−16] in manipulating electronic relaxation processes,[10,17,18,29] and even in realizing lasings from Bose−Einstein condensation.[19−22] An interesting applications has been found to enhance the reverse intersystem crossing (rISC) process, which is a decisive process for thermally activated delayed fluorescence (TADF) materials, the so-called third generation organic light-emitting diodes (OLEDs) with exciton utilization efficiency close to unity under current injection.[23−26]

There have been a number of studies about the polariton-enhanced rISC process for organic electronic devices.[18,27−29] The underlying mechanism has been under scrutiny. As pointed out by Martinez-Martinez et al., the rISC rate from T_1 to the lower polariton (LP) state inversely proportional to the effective number of molecules which coupled with the photon (denoted as N_{eff}), considering that the polariton is delocalized across N_{eff} singlet excitons and only one component can be effectively coupled to a given localized triplet exciton.[32,33] At the resonance condition, the effective number N_{eff} accounts for nearly 1/3 of the total number of molecules in the cavity.[32,33] In fact, the effective number of molecules inside a cavity can be as large as hundreds of thousands. The rISC rates are difficult

Received: August 18, 2022
Accepted: September 27, 2022

https://doi.org/10.1021/acs.jpclett.2c02557
J. Phys. Chem. Lett. 2022, 13, 9279−9286

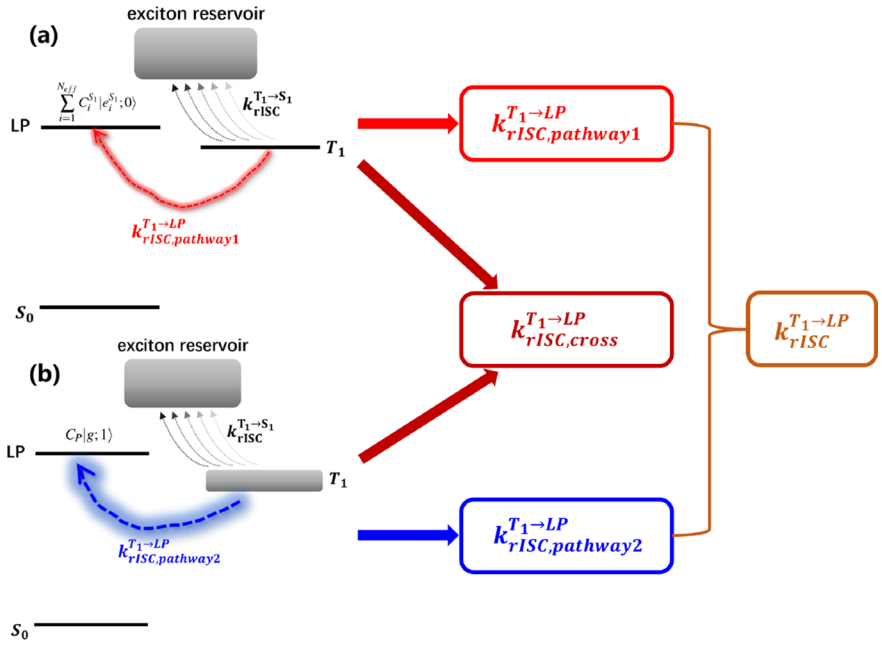

Figure 1. Schematic graph of three rISC channels. (a) rISC process from T_1 to the LP originated from spin−orbit coupling between T_1 and the exciton part of the LP (the rate constant is $k_{rISC,pathway1}^{T_1\rightarrow LP}$). (b) rISC process from T_1 to the LP originated from the LMC between T_1 and the photonic part of the LP (the rate constant is $k_{rISC,pathway2}^{T_1\rightarrow LP}$). Pathway1 and pathway2 together contribute to $k_{rISC,cross}^{T_1\rightarrow LP}$.

Table 1. Absorption/Emission Energies of S_1 and T_1, the 0−0 S_1−T_1 Energy Gap $\Delta E_{S_1T_1}^{0-0}$, and Various Rate Constants of DABNA-2

energetics	exptl (eV)[31]	calcd (eV)
S_1 absorption	2.817	2.83
S_1 emission	2.61	2.66
T_1 emission	2.46	2.46
$\Delta E_{S_1T_1}^{0-0}$	0.1960	0.2132
rate constants	**exptl (s^{-1})[31]**	**calcd (s^{-1})**
k_F	14.1×10^7	7.87×10^7
k_{nr,S_1}	1.6×10^7	4.1×10^7
k_{ISC}	10.1×10^6	1.73×10^6
k_{RISC}	14.8×10^3	1.44×10^3

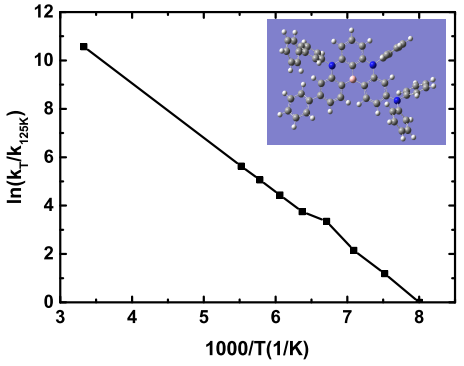

Figure 2. Relative rate change between S_1 and T_1 at different temperatures. The inset shows the chemical structure of DABNA-2.

to enhance except for the weak S_1−T_1 mixing of emitter and the transition of S_1−T_1 in the inverted Marcus regime, which have been theoretically studied.[32] The rISC process is typically a slow process, which is much longer than typical time span of

Table 2. Nonresonant Rabi-Splitting $\hbar\Omega_R^{nonres}$, the LMC between T_1 and the Intracavity Photon $\hbar\Omega_{T_1}$, the Energy of the LP E_{LP}, and the Photon Energy ε_P of Different Cavities, 0−0 LP−T_1 Energy Gap $\Delta E_{LP,T_1}^{0-0}$ at Different Cavities

cavity	$\hbar\Omega_R^{nonres}$ (eV)	$\hbar\Omega_{T_1}$ (cm^{-1})	E_{LP} (eV)	ε_P (eV)	$\Delta E_{LP,T_1}^{0-0}$ (meV)
cavity1	0.37	0.0914	2.49	2.69	150.6
cavity2	0.35	0.0907	2.48	2.65	132.5
cavity3	0.41	0.0872	2.35	2.45	10.0
cavity4	0.45	0.0854	2.28	2.35	−67.0

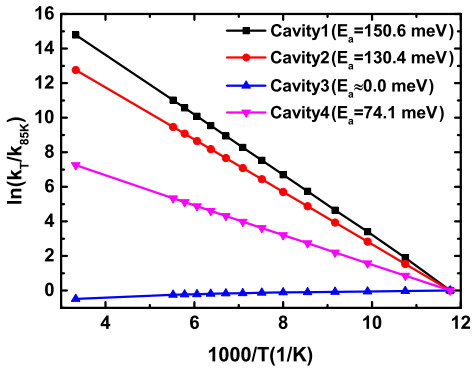

Figure 3. Relative rate change between the LP and T_1 at different temperatures.

excited state dynamics simulation.[35−37] So, the evaluation of rISC rate is a challenge for theoretical chemistry. Fortunately, the thermal vibration correlation function (TVCF) has become the useful approach to quantitatively calculate the ISC/rISC rate,[38−40] which has been successfully used to calculate the experimentally observed doping concentartion-dependent polariton-enhanced rISC rate in ErB (erythrosine B),[30] where it was found that the light−matter coupling (LMC)

https://doi.org/10.1021/acs.jpclett.2c02557
J. Phys. Chem. Lett. 2022, 13, 9279−9286

Table 3. RISC Rates in DABNA-2 ($k^{rISC}_{cav\text{-}out}$) and Cavities1-4 ($k^{rISC}_{cav1-cav4}$) at Different Temperatures

T/K	$k^{rISC}_{cav\text{-}out}$ (s^{-1})	k^{rISC}_{cav1} (s^{-1})	k^{rISC}_{cav2} (s^{-1})	k^{rISC}_{cav3} (10^7 s^{-1})	k^{rISC}_{cav4} (10^4 s^{-1})
125	0.037	0.367	2.278	0.817	1.528
133	0.122	0.849	4.721	0.800	2.311
141	0.317	1.792	9.008	0.784	3.336
149	1.060	3.479	16.044	0.772	4.631
157	1.580	6.315	26.942	0.755	6.221
165	3.130	10.816	43.023	0.744	8.125
173	5.850	17.621	65.797	0.727	10.357
181	10.30	27.491	96.911	0.716	12.926
300	1440.0	1189.7	2612.8	0.564	87.859

between T_1 and the intracavity photon dominate the total rISC rate for molecules with a non-negligible transition dipole moment (TDM) in the T_1 state such as for ErB. The theoretical results are in good agreement with the experimental data,[18] indicating that the LMC between T_1 and the intracavity photon has a significant promoting effect on enhancing the rISC rate of ErB.[30]

However, the above work only focuses on resonant cavities. Recently, it has been experimentally observed the detuning effects in the polariton-enhanced rISC process.[29] Both laser incident angle and cavity structure can lead to a detuning effect, deviating from the resonance. In this work, we focus on experimentally reported nonresonant cavities, i.e., the DABNA-2 molecule.[29] First, we develop a general rate formalism for the rISC transition from T_1 to the LP with full consideration of detuning effects. Then, we combine the novel formalism coupled with properly benchmarked electronic structure calculations to quantitatively investigate the experimentally observed barrier-free rISC process as a function of temperature. Finally, we investigate the influence of the laser incident angle and doping concentration on the barrier-free rISC process. The proposed formalism and mechanism provide a solid ground for molecular design toward highly efficient cavity-promoted light-emitting materials.

In this work, we use Fabry–Pérot cavity structure as employed in experimental work[29] to build a theoretical model. The incident light enters the cavity and is reflected many times to form a standing wave. Here, we simplify the intracavity electromagnetic field to a single photon. The photon energy in the cavity is determined by the incident light angle and the distance between the metal mirrors.[5,29] Based on the Tavis–Cummings model, we derive the rISC rate formulizm from T_1 to the LP (see the Supporting Information). Here, we study the system which is N identical molecules inside an optical cavity. The schematic graph is shown as Figure 1. When the LMC between S_1 and the intracavity photon is very strong, the coupling strength between the ith molecule and the intracavity photon $\hbar g_i$ can be written as[7,30]

$$\hbar g_i = |\vec{\mu}_{S_1}| \sqrt{\frac{\hbar\omega_c}{2\varepsilon_0\varepsilon_\infty V}} \cos\theta_i \tag{1}$$

where $\vec{\mu}_{S_1}$ is the transition dipole moment of the S_1 state, ω_c is the frequency of the intracavity photon, ε_∞ is the optical dielectric constant of the matrix inside the cavity, ε_0 is the

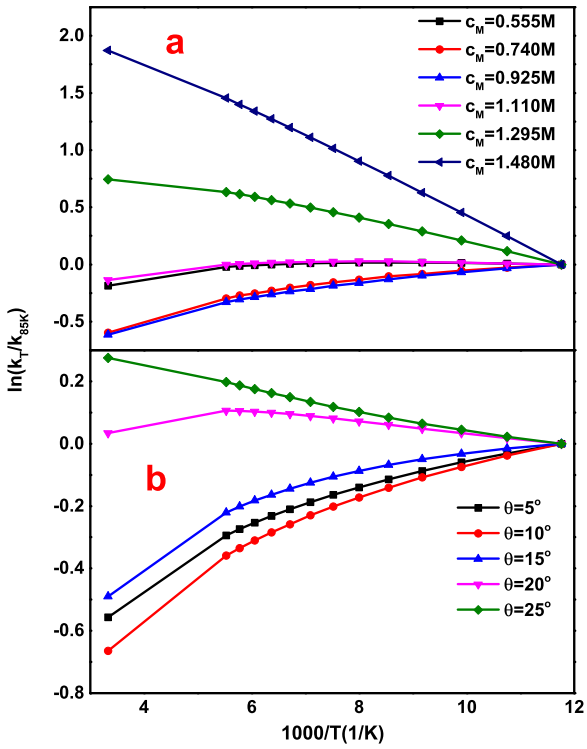

Figure 5. (a) Relative rate change from T_1 to the LP at different doping concentrations in cavity3. (b) Relative rate change from T_1 to the LP at different incident angles in cavity3.

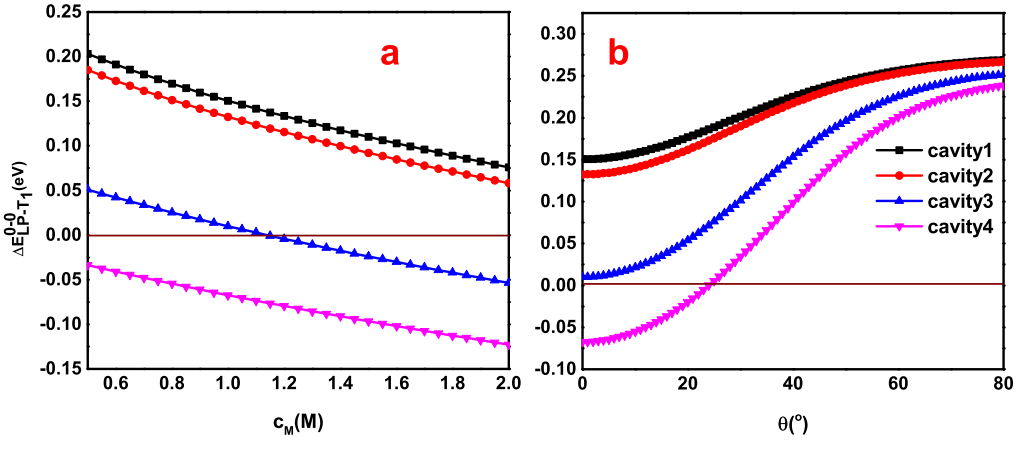

Figure 4. (a) LP energy in four cavities at different doping concentrations. (b) LP energy in four cavities at different incident angles.

https://doi.org/10.1021/acs.jpclett.2c02557
J. Phys. Chem. Lett. 2022, 13, 9279−9286

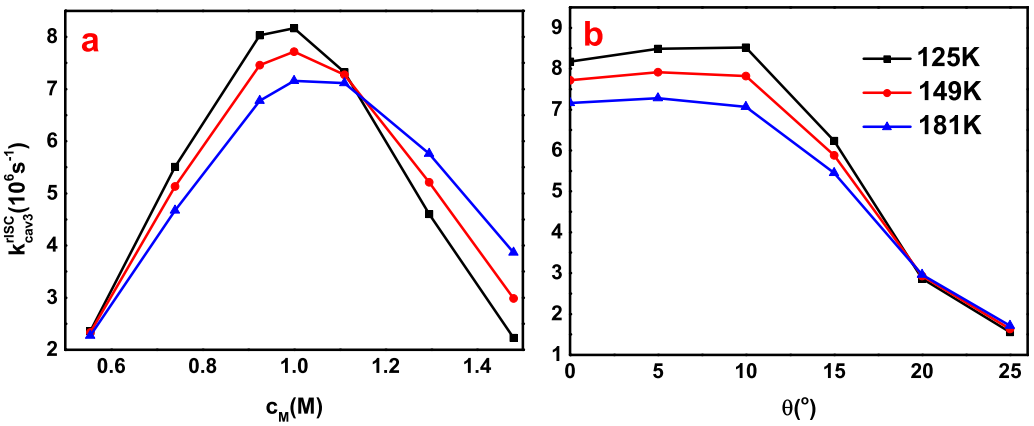

Figure 6. (a) rISC rates from T_1 to the LP at different doping concentrations in cavity3. (b) rISC rates from T_1 to the LP at different incident angles in cavity3.

vacuum permittivity, θ_i is the angle between the TDM of the ith S_1 and the intracavity photon, and V is the cavity mode volume.

Here, we ignore the exciton−exciton coupling among the S_1 states of N molecules. Under the strong LMC condition, there is one LP state, one upper polariton (UP) state, and $N - 1$ purely dark states (molecular excited states).[41] When the intracavity photon frequency is resonant with the energy of S_1 (which is the previous work of our group[30]), the energy difference between the LP and the UP is the resonant Rabi splitting $\hbar\Omega_R^{res}$, which can be written as

$$\hbar\Omega_R^{res} = 2\sqrt{\sum_i (\hbar g_i)^2} = 2|\vec{\mu}_{S_1}|\sqrt{\frac{\hbar\omega_c \sum_i \cos^2\theta_i}{2\varepsilon_0\varepsilon_\infty V}} \tag{2}$$

Within the random orientation model,[30] it becomes

$$\hbar\Omega_R^{res} = \frac{2}{\sqrt{3}}|\vec{\mu}_{S_1}|\sqrt{\frac{\hbar\omega_c c_M}{2\varepsilon_0\varepsilon_\infty}} \tag{3}$$

where c_M is the doping concentration of the molecule. The nonresonant Rabi-splitting $\hbar\Omega_R^{nonres}$ can be expressed as

$$\hbar\Omega_R^{nonres} = \sqrt{\frac{2}{3}|\vec{\mu}_{S_1}|^2\frac{\hbar\omega_c c_M}{\varepsilon_0\varepsilon_\infty} + (\hbar\omega_c - \varepsilon_{S_1})^2} \tag{4}$$

where ε_{S_1} is the energy of the S_1 state. The effective coupling $\sqrt{N_{eff}}\hbar\bar{g}_{S_1}$ can be written as

$$\sqrt{N_{eff}}\hbar\bar{g}_{S_1} = \frac{1}{\sqrt{3}}|\vec{\mu}_{S_1}|\sqrt{\frac{\hbar\omega_c c_M}{2\varepsilon_0\varepsilon_\infty}} \tag{5}$$

Previously,[30] we found that the coupling between T_1 and the photon component of the LP is dominant. If the TDM of T_1 is $\vec{\mu}_{T_1}$, the effective LMC between T_1 excitons and the intracavity photon can be written as

$$\hbar\Omega_{T_1} = \sqrt{N_{eff}}\hbar\bar{g}_{T_1} = \frac{1}{\sqrt{3}}|\vec{\mu}_{T_1}|\sqrt{\frac{\hbar\omega_c c_M}{2\varepsilon_0\varepsilon_\infty}} \tag{6}$$

Due to the TDM of the T_1 state $\vec{\mu}_{T_1}$ is much smaller than that of the S_1 state, and the LMC coupling between the T_1 state and the intracavity photon is very weak. So, the hybrid polaritonic triplet states cannot be formed. The frequency of the intracavity photon ω_c can be regulated by changing the incident angle in the following way[29]

$$\omega_c(\theta) = \frac{\omega_c(\theta = 0)}{\sqrt{1 - \left(\frac{\sin\theta}{n_{refract}}\right)^2}} \tag{7}$$

where θ is the incident angle and $n_{refract}$ is the refractive index. Based on the Tavis−Cummings model,[6] the LP state can be written as

$$|LP\rangle = C_p|g;\ 1\rangle + \sum_{i=1}^{N_{eff}} C_i^{S_1}|e_i^{S_1};\ 0\rangle \tag{8}$$

where $|0\rangle$ and $|1\rangle$ are the intracavity photonic states, $|g;\ 1\rangle$ is the state which represents all molecules in the ground state plus a intracavity photon, $|e_i^{S_1};\ 0\rangle$ is the state which represents the ith excited molecule plus cavity mode in vacuum state. The normalization condition is

$$\sum_{i=1}^{N_{eff}} |C_i^{S_1}|^2 + |C_p|^2 = 1 \tag{9}$$

The LP state is delocalized over N molecules and one intracavity photon, and $|C_p|^2$ represents the photonic component in the LP. The coefficient $C_i^{S_1}(i = 0, ..., N)$ depends on the detuning factor defined as the energy difference between the exciton and the intracavity photon. Based on the TVCF rate formalism and Fermi's golden rule (see the Supporting Information), the rISC rate between the LP and T_1 can be calculated as[23,42]

$$k_{rISC}^{T_1\to LP} = \left[\frac{\sum_{i=1}^{N_{eff}}|C_i^{S_1}|^2}{N_{eff}}(H_{if}^{SOC})^2 + 2\frac{|C_p|\sqrt{\sum_{i=1}^{N_{eff}}|C_i^{S_1}|^2}}{\sqrt{N_{eff}}} \times (\sqrt{N_{eff}}\hbar\bar{g}_{T_1})(H_{if}^{SOC}) + |C_p|^2(\sqrt{N_{eff}}\hbar\bar{g}_{T_1})^2\right] \times \int_{-\infty}^{\infty} dt\ e^{i\hbar\omega_{LP\text{-}T_1}t}\rho_{LP\text{-}T_1}(t, T) \tag{10}$$

where H_{if}^{SOC} is the SOC constant between T_1 and S_1, $\omega_{LP\text{-}T_1}$ is the frequency difference, and $\rho_{LP\text{-}T_1}(t, T)$ is the Franck−Condon factor between T_1 and the LP. The rISC process from

https://doi.org/10.1021/acs.jpclett.2c02557
J. Phys. Chem. Lett. 2022, 13, 9279−9286

T_1 to the LP can be triggered due to the strong LMC. Then, the rISC rate may be significantly changed. To compute the rISC rate constant from T_1 to the LP, the vibronic decoupling effect can be adopted when the Rabi frequency is larger than the highest frequency of vibrational modes coupled to the excited states.[33,43,44] According to the vibronic decoupling effect, the LP has the same vibrational structure as the ground state.[33,43,44] Hence, $\rho_{\text{LP-}T_1}(t, T)$ is replaced by $\rho_{\text{g-}T_1}(t, T)$, which is the Franck−Condon factor between the ground state and the T_1 state. Under the framework of the short-time and high-temperature approximation, the intersystem crossing rate can be expressed as

$$k_{\text{rISC}}^{T_1\rightarrow \text{LP}} \approx \frac{1}{\hbar^2}\left\{\frac{\sum_{i=1}^{N_{\text{eff}}}|C_i^{S_1}|^2}{N_{\text{eff}}}(H_{\text{if}}^{\text{SOC}})^2 + 2\frac{|C_{\text{P}}|\sqrt{\sum_{i=1}^{N_{\text{eff}}}|C_i^{S_1}|^2}}{\sqrt{N_{\text{eff}}}} \times (\sqrt{N_{\text{eff}}}\hbar\overline{g}_{T_1})(H_{\text{if}}^{\text{SOC}}) + |C_{\text{P}}|^2(\sqrt{N_{\text{eff}}}\hbar\overline{g}_{T_1})^2\right\} \times \sqrt{\frac{\pi}{\lambda_{\text{g-}T_1}k_{\text{B}}T}}\exp\left\{-\frac{(\Delta E_{\text{LP},T_1}^{0-0} - \lambda_{\text{g-}T_1})^2}{4\lambda_{\text{g-}T_1}k_{\text{B}}T}\right\} \tag{11}$$

which is the Marcus−Levich expression for the rISC rate.[23,34] Based on the vibronic decoupling effect, the rISC rate from T_1 to the LP which originated from spin−orbit coupling can be written as

$$k_{\text{rISC,pathway1}}^{T_1\rightarrow \text{LP}} = \frac{1}{\hbar^2}\left\{\frac{\sum_{i=1}^{N_{\text{eff}}}|C_i^{S_1}|^2}{N_{\text{eff}}}|H_{\text{if}}^{\text{SOC}}|^2\right\} \times \int_{-\infty}^{+\infty} \text{d}t\ \text{e}^{\text{i}\omega_{\text{LP-}T_1}t}\rho_{\text{g-}T_1}(t, T) \tag{12}$$

The mechanism of the SOC-triggered rISC process is schematically depicted in Figure 1 (a). It also can simplified to the Marcus−Levich equation

$$k_{\text{rISC,pathway1}}^{T_1\rightarrow \text{LP}} \approx \frac{1}{\hbar^2}\left\{\frac{\sum_{i=1}^{N_{\text{eff}}}|C_i^{S_1}|^2}{N_{\text{eff}}}|H_{\text{if}}^{\text{SOC}}|^2\right\} \times \sqrt{\frac{\pi}{\lambda_{\text{g-}T_1}k_{\text{B}}T}}\exp\left\{-\frac{(\Delta E_{\text{LP},T_1}^{0-0} - \lambda_{\text{g-}T_1})^2}{4\lambda_{\text{g-}T_1}k_{\text{B}}T}\right\} \tag{13}$$

The rISC process will be changed by the LMC between T_1 states and the intracavity photon if molecules have a non-negligible TDM of T_1. The rates can be written as

$$k_{\text{rISC,pathway2}}^{T_1\rightarrow \text{LP}} = \frac{1}{\hbar^2}\{|C_{\text{P}}|^2|\hbar\Omega_{T_1}|^2\}\int_{-\infty}^{+\infty}\text{d}t\ \text{e}^{\text{i}\omega_{\text{LP-}T_1}t}\rho_{\text{g-}T_1}(t, T) \tag{14}$$

The mechanism of the LMC-triggered rISC process is schematically depicted in Figure 1 (b). It can be also simplified to the Marcus−Levich type of expression:

$$k_{\text{rISC,pathway2}}^{T_1\rightarrow \text{LP}} \approx \frac{1}{\hbar^2}\{|C_{\text{P}}|^2|\hbar\Omega_{T_1}|^2\} \times \sqrt{\frac{\pi}{\lambda_{\text{g-}T_1}k_{\text{B}}T}}\exp\left\{-\frac{(\Delta E_{\text{LP},T_1}^{0-0} - \lambda_{\text{g-}T_1})^2}{4\lambda_{\text{g-}T_1}k_{\text{B}}T}\right\} \tag{15}$$

In addition to $k_{\text{rISC,pathway1}}^{T_1\rightarrow \text{LP}}$ and $k_{\text{rISC,pathway2}}^{T_1\rightarrow \text{LP}}$, there is a cross-term $k_{\text{rISC,cross}}^{T_1\rightarrow \text{LP}}$ in $k_{\text{rISC}}^{T_1\rightarrow \text{LP}}$

$$k_{\text{rISC,cross}}^{T_1\rightarrow \text{LP}} = \frac{2}{\hbar^2}\left\{\frac{|C_{\text{P}}|\sqrt{\sum_{i=1}^{N_{\text{eff}}}|C_i^{S_1}|^2}}{\sqrt{N_{\text{eff}}}}(\sqrt{N_{\text{eff}}}\hbar\overline{g}_{T_1})(H_{\text{if}}^{\text{SOC}})\right\} \times \int_{-\infty}^{+\infty}\text{d}t\ \text{e}^{\text{i}\omega_{\text{LP-}T_1}t}\rho_{\text{g-}T_1}(t, T) \tag{16}$$

Single Molecular Properties of DABNA-2. Molecular geometries for DABNA-2 are optimized by density functional theory (DFT) for ground state S_0 and by time-dependent DFT (TDDFT) for S_1 and T_1 states, both with B3LYP/def2-svp. Since TD-B3LYP/def2-svp cannot provide the accurate value for the S_1−T_1 energy gap for the multiresonant (MR) TADF systems such as DABNA-2, we apply SCS-CC2 (second-order approximate coupled cluster) to evaluate $\Delta E_{S_1T_1}$ while keeping TD-B3LYP/def2-svp for calculating the excitation energy of S_1) to balance the accuracy and cost.[45] From Table 1, we can see that the excitation energies calculated by TDDFT/B3LYP are consistent with the experimental results. Explicit values of the TDM of S_1/T_1, the SOC between S_1 and T_1 for DABNA-2, the computational details, are given in the Supporting Information.

Based on the knowledge of electronic structure, we compute the rate constants of different physical processes by the TVCF rate formalism.[38−40] The calculated results are listed in Table 1. For comparison, the experimental results[31] are also listed in Table 1. The overall agreement between the calculated rate constants and the corresponding experimental results rationalizes the electronic structure parameters and the TVCF rate formalism. Next, we will study the change of the rISC process in respect of temperature. The rISC process is a thermally activated process, and the relative rate change is linearly dependent on temperature.[23,34] Experimentally, the relative rate change with respect to the different temperatures has been observed within a wide temperature range (from 77 to 181 K). Theoretically, k_{rISC} of DABNA-2 at different temperatures has been calculated, and the results are shown in Figure 2. As shown in Figure 2, the relative rate change is linearly dependent on temperature (from 125 to 300 K). The energy barrier can be calculated according to the Arrehenius law:

$$\ln(k_T/k_{T_0}) = -\frac{E_{\text{a}}}{1000k_{\text{B}}}\left(\frac{1000}{T} - \frac{1000}{T_0}\right) \tag{17}$$

where $k_T(k_{T_0})$, k_{B}, and E_{a} correspond to the rISC rate at the temperature T (T_0), the Boltzmann constant, and the energy barrier. The calculated results (E_{a} = 192.9 meV) are slightly larger than experimental results (E_{a} = 115.0 meV), which may be caused by the fact that the zero point energy $\Delta E_{S_1T_1}^{0-0}$ of the experiment is 0.14 eV.[29] The overall tendency of the rISC rates of DABNA-2 can be qualitatively reproduced. The agreement between the calculated rISC rates and the corresponding experimental results rationalizes our extended rISC rate theory. Based on the electronic structure parameters and the extended rISC rate theory, we can further explore the rISC process inside the cavity.

The rISC Process Inside the Cavity. Based on the single molecular properties of DABNA-2, we further calculate the light−matter coupling of DABNA-2 and the intracavity photon

https://doi.org/10.1021/acs.jpclett.2c02557
J. Phys. Chem. Lett. 2022, 13, 9279−9286

at different temperature based on the setup experiments.[29] The ε_∞ of toluene is the square of $n_{refract}$ = 1.541 ($\varepsilon_\infty = n_{refract}^2 = 2.375$).[29,46] From Table 2, we can see that the Rabi splitting $\hbar\Omega_R^{nonres}$ is large enough for different cavities, and then the LP and UP states can be formed. In addition, it is in accord with the experimental absorption spectra.[29] Meanwhile, it is difficult to calculate the effective number N_{eff} because of the absence of the intracavity photon density, which should be provided by relevant experiment. Here, we fix the width and length of the optical cavity as two times as large as the experimentally measured thickness of the doped film (130 nm) to express volume V, i.e., 130 nm × 260 nm × 260 nm, and the doping concentration c_M = 1.0 M. N is 5.28 × 10^6 based on $N = c_M V N_A$, where N_A is the Avogadro constant, and the effective number of molecules N_{eff} ($N_{eff} = N/3$) is 1.76 × 10^6, which has a similar order of magnitude with the results estimated in refs 30 and 33.

$$\ln(k_T/k_{T_0}) = \frac{1}{2}\ln(T_0/T) - \frac{(\Delta E_{LP,T_1}^{0-0} - \lambda_{g\text{-}T_1})^2}{4\lambda_{g\text{-}T_1}(1000k_B)}\left(\frac{1000}{T} - \frac{1000}{T_0}\right) \quad (18)$$

The LMC coupling between T_1 and the intracavity photon is much smaller than that between S_1 and the intracavity photon. So, the T_1 state cannot participate in the formation of the LP for all cavities, which is in accord with the experimental result[29] that the phosphorescence spectra remain much the same for inside and outside cavity. However, the LMC coupling between T_1 and photon may trigger the rISC process from T_1 to the LP. From Table 2, the zero point energy $\Delta E_{LP,T_1}^{0-0}$ is different for all cavities, which triggers different rISC process between the LP and T_1. Theoretically, the relative rate change $\ln(k_T/k_{85K})$ at different temperatures has been calculated, and the results are shown in Figure 3. The calculated values are shown in Table 3. Because the $\Delta E_{LP,T_1}^{0-0}$ values of cavity1 and cavity2 are very large, the rISC process from T_1 to the LP is a thermally activated process, the energy barrier E_a of cavity1 and cavity2 equals 150.6 and 130.4 meV, which are smaller than that for the cavity-free case. Amazingly, the zero point energy $\Delta E_{LP,T_1}^{0-0}$ is nearly zero, and the process becomes a barrier-free crossing from T_1 to the LP, in agreement with the experimental results.[29] It can be understood in an easier way from the Marcus−Levich equation (see eq 10). Namely, the nuclear quantum tunneling effect can promote the electron transfer process.[23,34] From Table 3, we can see that the rISC rates of cavity3 far outweigh those of other cavities and isolated DABNA-2. For cavity4, $\Delta E_{LP,T_1}^{0-0}$ is negative, and the rISC process again becomes a thermally activated process. Meanwhile, we calculate the $k_{pathway2}^{rISC}/k_{T_1\to LP}^{rISC}$ of different cavities. The values of cavity1, cavity2, cavity3, and cavity4 equal 99.819%, 99.837%, 99.902%, and 99.922%. The calculated results are shown in Table S3. So, we think that the rISC process arising from the LMC between T_1 and the photonic component of the LP is also very important for the typical TADF molecule (such as DABNA-2). In order to compare with the nonresonant cavities, we calculated the rISC rate constant of the resonant cavity, shown in Figure S1 (see the Supporting Information). We can see that it is difficult to reach the barrier-free process by increasing doping concentration c_M inside the resonant cavity. Only when c_M reaches a very high concentration (1.295 or 1.48 M) can a barrier-free process occur. This manifests the advantage of nonresonant cavities.

Next, we consider the influences of doping concentrations and incident angles on the enhancements of rISC rate. From eq 16, we can see that the cross-term depends on $\sqrt{N_{eff}}$. The concentration may affect its proportion in the total rate. Here, we calculate the $k_{pathway1}^{rISC}/k_{T_1\to LP}^{rISC}$, $k_{cross}^{rISC}/k_{T_1\to LP}^{rISC}$, and $k_{pathway2}^{rISC}/k_{T_1\to LP}^{rISC}$ at different concentrations in cavity3. The results are shown in Table S4. From Table S4, we can see that concentration indeed affects the ratio of $k_{cross}^{rISC}/k_{T_1\to LP}^{rISC}$. However, the cross-term does not dominate the total rate for any concentration. So, the rISC rate is largely dominated by the light−matter coupling between T_1 and the photonic part of the LP for DABNA-2. The relative rate change $\ln(k_T/k_{85K})$ at different doping concentrations c_M has been calculated, and the results are shown in Figure 5a. It decreases with the concentration c_M increasing from 0.555 to 0.925 M. However, the relative rate change decreases as the concentration c_M increases from 0.925 to 1.480 M. In addition, the rISC process changes from a barrier-free quantum tunneling process to a thermally activated process as the concentration increases. The calculated results of the relative rate change $\ln(k_T/k_{85K})$ at different incident angles θ are shown in Figure 5b. The relative rate change decreases as θ increases from 5° to 10°. However, the relative rate change decreases as the incident angle increases from 10° to 25°. In addition, the rISC process undergoes a transition from a barrier-free quantum tunneling process to a thermally activated process as θ increases.

From Figure 6, we can see that the barrier-free rISC rates exhibit a maximum as θ and c_M change. k_{cav3}^{rISC} first increases and then decreases with the increase of c_M (or θ), which shows a parabolic-shape dependence. The phenomena can be understood via the relation between the zero-point energy difference $\Delta E_{LP,T_1}^{0-0}$ and c_M (or θ). From Figure 4a, we can see that $\Delta E_{LP,T_1}^{0-0}$ first decreases to zero and then becomes negative with the increase of c_M, leading to k_{cav3}^{rISC} showing a parabolic-shape dependence (see eq 11). Figure 4b shows that $\Delta E_{LP,T_1}^{0-0}$ monotonically increases with the increase of θ, and the starting point is very close to zero (10.0 meV). However, $\frac{(\Delta E_{LP,T_1}^{0-0} - \lambda_{g\text{-}T_1})^2}{4\lambda_{g\text{-}T_1}}$ ($\lambda_{g\text{-}T_1}$ = 753.16 cm^{-1}) first decreases to zero and then increases with the increase of θ, leading to k_{cav3}^{rISC} showing a parabolic-shape dependence (see eq 11). Perhaps $\frac{(\Delta E_{LP,T_1}^{0-0} - \lambda_{g\text{-}T_1})^2}{4\lambda_{g\text{-}T_1}}$ can be used as a good descriptor to characterize the rISC (from T_1 to the LP) performance. The descriptor remains for future investigations.

To conclude, we have derived a comprehensive rISC rate formalism with consideration of contributions from spin−orbit coupling between T_1 and the excitonic part of the LP, light−matter coupling between T_1 and the photonic part of the LP, and their cross-term. The second term is found to be overwhelmingly dominant. The rate formalism is applied to investigate the detuning effect for rISC process in MR-TADF material. The following conclusions are drawn: (i) The relative rate change of DABNA-2 inside different cavities which is the experimentally observed can be reproduced that the enhanced rISC of DABNA-2 inside the cavity can be effectively promoted by the LMC between its T_1 and the intracavity

https://doi.org/10.1021/acs.jpclett.2c02557
J. Phys. Chem. Lett. 2022, 13, 9279−9286

photon. (ii) The rISC rate from T_1 to the LP can be enhanced by orders of magnitudes through detuning effect to lower the transition barrier, even reaching barrier-free maximum through manipulating the light incident angle and dopant concentration. The latter determines the detuning energy, namely, the difference between the LP and T_1. Our work provided a theoretical protocol for evaluating the rate processes for the molecular aggregate in the microcavity, and the experimental findings of the barrier-free rISC process in DABNA-2 have been explained by the detuning effect.

■ ASSOCIATED CONTENT

Supporting Information

The Supporting Information is available free of charge at https://pubs.acs.org/doi/10.1021/acs.jpclett.2c02557.

Derivation of the rISC rate formula from T_1 to the LP, experimental and calculated polariton-enhanced rISC rates of ErB with respect to different doping concentrations, TDM of S_1 and T_1 of DABNA-2, SOC between S_1 and T_1 of DABNA-2, computational details, polariton-enhanced rISC rates of DABNA-2 with respect to different cavities at 300 K, $k^{rISC}_{pathway1}/k^{rISC}_{T_1\rightarrow LP}$, $k^{rISC}_{cross}/k^{rISC}_{T_1\rightarrow LP}$ and $k^{rISC}_{pathway2}/k^{rISC}_{T_1\rightarrow LP}$ of DABNA-2 with respect to different doping concentrations c_M in cavity3, the relative rate change between the LP and T_1 at different doping concentrations in resonant cavity (PDF)

■ AUTHOR INFORMATION

Corresponding Author

Zhigang Shuai − *MOE Key Laboratory of Organic OptoElectronics and Molecular Engineering, Department of Chemistry, Tsinghua University, Beijing 100084, P R China; School of Science and Engineering, The Chinese University of Hong Kong, Shenzhen, Guangdong 517128, P R China;* orcid.org/0000-0003-3867-2331; Email: zgshuai@tsinghua.edu.cn

Author

Bin Zhang − *MOE Key Laboratory of Organic OptoElectronics and Molecular Engineering, Department of Chemistry, Tsinghua University, Beijing 100084, China;* orcid.org/0000-0002-0170-2923

Complete contact information is available at: https://pubs.acs.org/10.1021/acs.jpclett.2c02557

Notes

The authors declare no competing financial interest.

■ ACKNOWLEDGMENTS

Financial support from the National Natural Science Foundation of China (Grant Nos. 21788102) as well as the Ministry of Science and Technology of China through the National Key R&D Plan (Grant No. 2017YFA0204501) is gratefully acknowledged.

■ REFERENCES

(1) Peng, Q.; Shuai, Z. G. Molecular mechanism of aggregation-induced emission. *Aggregate* **2021**, *2* (5), No. e91.

(2) Han, G. C.; Yi, Y. P.; Shuai, Z. G. From Molecular Packing Structures to Electronic Processes: Theoretical Simulations for Organic Solar Cells. *Adv. Energy. Mater.* **2018**, *8* (28), 1702743.

(3) Liu, R.; Ge, Y. F.; Wang, D.; Shuai, Z. G. Understanding the Temperature Dependence of the Seebeck Coefficient from First-Principles Band Structure Calculations for Organic Thermoelectric Materials. *CCS Chem.* **2021**, *3*, 1477.

(4) Keeling, J.; Kéna-Cohen, S. Bose−Einstein Condensation of Exciton-Polaritons in Organic Microcavities. *Annu. Rev. Phys. Chem.* **2020**, *71*, 435−459.

(5) Hertzog, M.; Wang, M.; Mony, J.; Börjesson, K. Strong Light-Matter Interactions: A New Direction within Chemistry. *Chem. Soc. Rev.* **2019**, *48*, 937−961.

(6) Ribeiro, R. F.; Martínez-Martínez, L. A.; Du, M.; Campos-Gonzalez-Angulo, J.; Yuen-Zhou, J. Polariton Chemistry: Controlling Molecular Dynamics with Optical Cavities. *Chem. Sci.* **2018**, *9*, 6325−6339.

(7) Ebbesen, T. W. Hybrid Light-Matter States in a Molecular and Material Science Perspective. *Acc. Chem. Res.* **2016**, *49*, 2403−2412.

(8) Dovzhenko, D. S.; Ryabchuk, S. V.; Rakovich, Y. P.; Nabiev, I. R. Light-Matter Interaction in the Strong Coupling Regime: Configurations, Conditions, and Applications. *Nanoscale* **2018**, *10*, 3589−3605.

(9) Schwartz, T.; Hutchison, J. A.; Genet, C.; Ebbesen, T. W. Reversible Switching of Ultrastrong Light-Molecule Coupling. *Phys. Rev. Lett.* **2011**, *106*, 196405.

(10) Hutchison, J. A.; Schwartz, T.; Genet, C.; Devaux, E.; Ebbesen, T. W. Modifying Chemical Landscapes by Coupling to Vacuum Fields. *Angew. Chem., Int. Ed.* **2012**, *51*, 1592−1596.

(11) Galego, J.; Garcia-Vidal, F. J.; Feist, J. Many-Molecule Reaction Triggered by a Single Photon in Polaritonic Chemistry. *Phys. Rev. Lett.* **2017**, *119*, 136001.

(12) Munkhbat, B.; Wersäll, M.; Baranov, D. G.; Antosiewicz, T. J.; Shegai, T. Suppression of Photo-Oxidation of Organic Chromophores by Strong Coupling to Plasmonic Nanoantennas. *Sci. Adv.* **2018**, *4*, No. eaas9552.

(13) Coles, D. M.; Niccolo Somaschi, P. M.; Clark, C.; Lagoudakis, P. G.; Savvidis, P. G.; Lidzey, D. G. Polariton-Mediated Energy Transfer between Organic Dyes in a Strongly Coupled Optical Microcavity. *Nat. Mater.* **2014**, *13*, 712−719.

(14) Zhong, X.; Chervy, T.; Wang, S.; George, J.; Thomas, A.; Hutchison, J. A.; Devaux, E.; Genet, C.; Ebbesen, T. W. Non-Radiative Energy Transfer Mediated by Hybrid Light-Matter States. *Angew. Chem., Int. Ed.* **2016**, *55*, 6202−6206.

(15) Zhong, X.; Chervy, T.; Zhang, L.; Thomas, A.; George, J.; Genet, C.; Hutchison, J. A.; Ebbesen, T. W. Energy Transfer between Spatially Separated Entangled Molecules. *Angew. Chem., Int. Ed.* **2017**, *56*, 9034−9038.

(16) Georgiou, K.; Michetti, P.; Gai, L.; Cavazzini, M.; Shen, Z.; Lidzey, D. G. Control over Energy Transfer between Fluorescent BODIPY Dyes in a Strongly Coupled Microcavity. *ACS Photonics* **2018**, *5*, 258−266.

(17) Kéna-Cohen, S.; Forrest, S. R. Green Polariton Photoluminescence Using the Red-Emitting Phosphor PtOEP. *Phys. Rev. B: Condens. Matter Mater. Phys.* **2007**, *76*, 075202.

(18) Stranius, K.; Hertzog, M.; Börjesson, K. Selective Manipulation of Electronically Excited States through Strong Light-Matter Interactions. *Nat. Commun.* **2018**, *9*, 2273.

(19) Kéna-Cohen, S.; Forrest, S. R. Room-temperature polariton lasing in an organic single-crystal microcavity. *Nat. Photonics* **2010**, *4*, 371−375.

(20) Bittner, E. R.; Silva, C. Estimating the Conditions for Polariton Condensation in Organic Thin-Film Microcavities. *J. Chem. Phys.* **2012**, *136*, 034510.

(21) Daskalakis, K. S.; Maier, S. A.; Murray, R.; Kéna-Cohen, S. Nonlinear Interactions in An Organic Polariton Condensate. *Nat. Mater.* **2014**, *13*, 271−278.

(22) Paschos, G. G.; Somaschi, N.; Tsintzos, S. I.; Coles, D.; Bricks, J. L.; Hatzopoulos, Z.; Lidzey, D. G.; Lagoudakis, P. G.; Savvidist, P.

G. Hybrid Organic-Inorganic Polariton Laser. *Sci. Rep.* **2017**, *7*, 11377.
(23) Peng, Q.; Fan, D.; Duan, R.; Yi, Y.; Niu, Y.; Wang, D.; Shuai, Z. Theoretical Study of Conversion and Decay Processes of Excited Triplet and Singlet States in a Thermally Activated Delayed Fluorescence Molecule. *J. Phys. Chem. C* **2017**, *121*, 13448−13456.
(24) Xu, S.; Yang, Q.; Wan, Y.; Chen, R.; Wang, S.; Si, Y.; Yang, B.; Liu, D.; Zheng, C.; Huang, W. Predicting Intersystem Crossing Efficiencies of Organic Molecules for Efficient Thermally Activated Delayed Fluorescence. *J. Mater. Chem. C* **2019**, *7*, 9523−9530.
(25) Cui, L.-S.; Gillett, A. J.; Zhang, S.-F.; Ye, H.; Liu, Y.; Chen, X.-K.; Lin, Z.-S.; Evans, E. W.; Myers, W. K.; Ronson, T. K.; Nakanotani, H.; Reineke, S.; Bredas, J.-L.; Adachi, C.; Friend, R. H. Fast Spin-Flip Enables Efficient and Stable Organic Electroluminescence from Charge-Transfer States. *Nat. Photonics* **2020**, *14*, 636−642.
(26) Zhan, X.; Wu, Z.; Gong, Y.; Tu, J.; Xie, Y.; Peng, Q.; Ma, D.; Li, Q.; Li, Z. Utilizing Electroplex Emission to Achieve External Quantum Efficiency up to 18.1% in Nondoped Blue OLED. *Research* **2020**, *2020*, 8649102.
(27) Xu, J.; Tang, X.; Zhao, X.; Zhu, H.; Qu, F.; Xiong, Z. Abnormal Reverse Intersystem Crossing of Polaron-Pair States and Its Conversion to Intersystem Crossing via the Regulation of Intermolecular Electron-Hole Spacing Distance. *Phys. Rev. Appl.* **2020**, *14*, 024011.
(28) Polak, D.; et al. Manipulating Molecules with Strong Coupling: Harvesting Triplet Excitons in Organic Exciton Microcavities. *Chem. Sci.* **2020**, *11*, 343−354.
(29) Yu, Y.; Mallick, S.; Wang, M.; Börjesson, K. Barrier-Free Reverse-Intersystem Crossing in Organic Molecules by Strong Light-Matter Coupling. *Nat. Commun.* **2021**, *12*, 3255.
(30) Ou, Q.; Shao, Y.; Shuai, Z. Enhanced Reverse Intersystem Crossing Promoted by Triplet Exciton-Photon Coupling. *J. Am. Chem. Soc.* **2021**, *143*, 17786−17792.
(31) Hatakeyama, T.; Shiren, K.; Nakajima, K.; Nomura, S.; Nakatsuka, S.; Kinoshita, K.; Ni, J.; Ono, Y.; Ikuta, T. Ultrapure Blue Thermally Activated Delayed Fluorescence Molecules: Efficient HOMO-LUMO Separation by the Multiple Resonance Effect. *Adv. Mater.* **2016**, *28*, 2777−2781.
(32) Martínez-Martínez, L. A.; Eizner, E.; Kéna-Cohen, S.; Yuen-Zhou, J. Triplet Harvesting in the Polaritonic Regime: A Variational Polaron Approach. *J. Chem. Phys.* **2019**, *151*, 054106.
(33) Eizner, E.; Martínez-Martínez, L. A.; Yuen-Zhou, J.; Kéna-Cohen, S. Inverting Singlet and Triplet Excited States Using Strong Light-Matter Coupling. *Sci. Adv.* **2019**, *5*, No. eaax4482.
(34) Wang, L.; Ou, Q.; Peng, Q.; Shuai, Z. Theoretical Characterizations of TADF Materials: Roles of ΔG and the Singlet-Triplet Excited States Interconversion. *J. Phys. Chem. A* **2021**, *125*, 1468−1475.
(35) Koch, A.; Kinzel, D.; Dröge, F.; Gräfe, S.; Kupfer, S. Photochemistry and Electron Transfer Kinetics in a Photocatalyst Model Assessed by Marcus Theory and Quantum Dynamics. *J. Phys. Chem. C* **2017**, *121*, 16066−16078.
(36) Menger, M. F. S. J.; Plasser, F.; Mennucci, B.; González, L. Surface Hopping within an Exciton Picture. An Electrostatic Embedding Scheme. *J. Chem. Theory Comput.* **2018**, *14*, 6139−6148.
(37) Westermayr, J.; Gastegger, M.; Menger, M. F. S. J.; Mai, S.; González, L.; Marquetand, P. Machine Learning Enables Long Time Scale Molecular Photodynamics Simulations. *Chem. Sci.* **2019**, *10*, 8100−8107.
(38) Shuai, Z.; Peng, Q. Excited States Structure and Processes: Understanding Organic Light-Emitting Diodes at the Molecular Level. *Phys. Rep.* **2014**, *537*, 123−156.
(39) Wang, Y.; Peng, Q.; Ou, Q.; Lin, S.; Shuai, Z. A Novel Molecular Descriptor for Highly Efficient (Φ_{TADF} > 90%) Transition Metal TADF Au(iii) Complexes. *J. Mater. Chem. A* **2020**, *8*, 18721−18725.
(40) Lin, S.; Ou, Q.; Wang, Y.; Peng, Q.; Shuai, Z. Aggregation-Enhanced Thermally Activated Delayed Fluorescence Efficiency for Two-Coordinate Carbene-Metal-Amide Complexes: A QM/MM Study. *J. Phys. Chem. Lett.* **2021**, *12*, 2944−2953.
(41) Houdré, R.; Stanley, R. P.; Ilegems, M. Vacuum-Field Rabi Splitting in the Presence of Inhomogeneous Broadening: Resolution of a Homogeneous Linewidth in an Inhomogeneously Broadened System. *Phys. Rev. A: At., Mol., Opt. Phys.* **1996**, *53*, 2711−2715.
(42) Niu, Y.; Peng, Q.; Deng, C.; Gao, X.; Shuai, Z. Theory of Excited State Decays and Optical Spectra: Application to Polyatomic Molecules. *J. Phys. Chem. A* **2010**, *114*, 7817−7831.
(43) Spano, F. C. Optical Microcavities Enhance the Exciton Coherence Length and Eliminate Vibronic Coupling in J-Aggregates. *J. Chem. Phys.* **2015**, *142*, 184707.
(44) Herrera, F.; Spano, F. C. Cavity-Controlled Chemistry in Molecular Ensembles. *Phys. Rev. Lett.* **2016**, *116*, 238301.
(45) Pershin, A.; Hall, D.; Lemaur, V.; Sancho-Garcia, J. C.; Muccioli, L.; Zysman-Colman, E.; Beljonne, D.; Olivier, Y. Highly emissive excitons with reduced exchange energy in thermally activated delayed fluorescent molecules. *Nat. Commun.* **2019**, *10*, 597.
(46) Robertson, J. In *Comprehensive Semiconductor Science and Technology*; Bhattacharya, P., Fornari, R., Kamimura, H., Eds.; Elsevier: Amsterdam, 2011; pp 132−176.

https://doi.org/10.1021/acs.jpclett.2c02557
J. Phys. Chem. Lett. 2022, 13, 9279−9286